




Intrinsic versus extrinsic orbital and electronic reconstructions at complex oxide interfaces

R. J. Green ^{1,2,*} V. Zabolotnyy,³ M. Zwiebler,⁴ Z. Liao,^{5,6} S. Macke,^{1,7} R. Sutarto,⁸ F. He,⁸ M. Huijben ⁵ G. Rijnders,⁵ G. Koster,⁵ J. Geck,⁴ V. Hinkov ³ and G. A. Sawatzky¹

¹Stewart Blusson Quantum Matter Institute, University of British Columbia, Vancouver, Canada V6T 1Z1

²Department of Physics & Engineering Physics, University of Saskatchewan, Saskatoon, Canada S7N 5E2

³Experimentelle Physik IV and Röntgen Research Center for Complex Materials (RCCM),

Fakultät für Physik und Astronomie, Universität Würzburg, Am Hubland, D-97074 Würzburg, Germany

⁴Institute for Structure Physics, Dresden Technical University, 01062 Dresden, Germany

⁵Faculty of Science and Technology and MESA+ Institute for Nanotechnology,

University of Twente, 7500 AE Enschede, The Netherlands

⁶National Synchrotron Radiation Laboratory, University of Science and Technology of China,

Hefei 230026, Anhui, China

⁷Max Planck Institute for Solid State Research, Heisenbergstraße 1, 70569 Stuttgart, Germany

⁸Canadian Light Source, University of Saskatchewan, Saskatoon, Canada SK S7N 2V3



(Received 15 March 2021; revised 2 June 2021; accepted 22 June 2021; published 29 June 2021)

The interface between the insulators LaAlO₃ (LAO) and SrTiO₃ accommodates a two-dimensional electron liquid (2DEL)—a high-mobility electron system exhibiting superconductivity as well as indications of magnetism and correlations. While this flagship oxide heterostructure shows promise for electronics applications, the origin and microscopic properties of the 2DEL remain unclear. The uncertainty remains in part because the electronic structures of such nanoscale-buried interfaces are difficult to probe and is compounded by the variable presence of oxygen vacancies and coexistence of both localized and delocalized charges. These various complications have precluded decisive tests of intrinsic electronic and orbital reconstruction at this interface. Here we overcome prior difficulties by developing an interface analysis based on the inherently interface-sensitive resonant x-ray reflectometry. We discover a high-charge density of 0.5 electrons per interfacial unit cell (u.c.) for samples above the critical LAO thickness and extract the depth dependence of both the orbital and the electronic reconstructions near the buried interface. We find that the majority of the reconstruction phenomena are confined to within 2 u.c. of the interface, and we quantify how oxygen vacancies significantly affect the electronic system. Our results provide strong support for the existence of polarity-induced electronic reconstruction, clearly separating its effects from those of oxygen vacancies.

DOI: [10.1103/PhysRevMaterials.5.065004](https://doi.org/10.1103/PhysRevMaterials.5.065004)

I. INTRODUCTION

The complex interplay between charge, spin, orbital, and lattice degrees of freedom in transition metal oxides leads to a multitude of emergent phenomena having numerous potential applications [1]. Often the phenomena are realized through explicit fine tuning of these degrees of freedom, for example, via electronic doping or applied pressure. Recent advances in atomic scale oxide thin film growth have yielded a new method of precisely tuning material properties via heterostructuring, where sequences of films are grown epitaxially on top of specially chosen substrates [2,3]. Orbital, spin, and electronic reconstructions, which can occur at the atomically precise interfaces, lead to emergent properties that are often very different from the corresponding bulk materials [3].

The interface between LaAlO₃ and SrTiO₃ (LAO/STO) is paradigmatic of the oxide heterostructure field, hosting

a two-dimensional electron liquid (2DEL) [4,5] that exhibits gate-tunable superconductivity [6–11], flexoelectricity [12], magnetism [13–15], and correlations [16,17]. Recent experiments have further utilized this interface as a foundation for the construction of 1D superconducting electron waveguides [7,18,19] which have potential application in quantum computing. However, while the system exhibits such fascinating properties and shows such promise for device applications [2], uncertainty remains regarding the origin and physical details of this highly studied interfacial electronic liquid [20]. Some of the earliest studies of the interface 2DEL [21] proposed that it results from an electronic reconstruction due to a *polar catastrophe*—that a diverging electric potential originating from charged LaO⁺ and AlO₂⁻ layers is rectified through a spontaneous relocation of 0.5 e⁻ per square unit cell (u.c.) from the LAO surface to the interface for heterostructures with LAO thicknesses greater than 3 u.c., thus forming the 2DEL. The concept of electronic reconstruction had been introduced several years earlier in studies of polar surfaces [22]. Crucially, however, transport measurements on LAO/STO typically find about an order of magnitude less

*robert.green@usask.ca

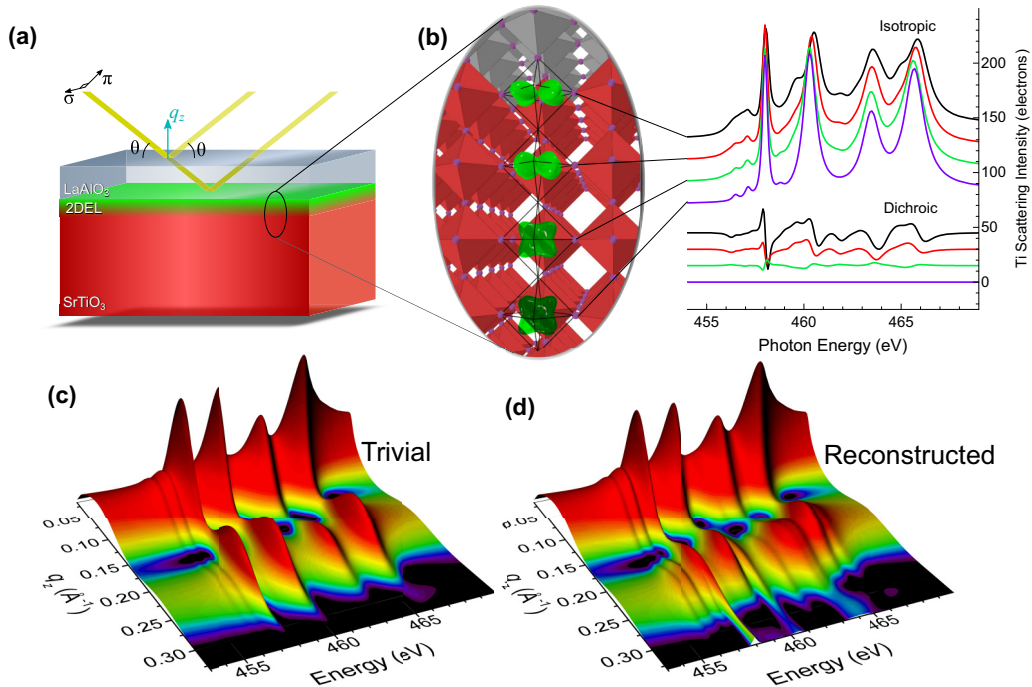


FIG. 1. Theoretical resonant reflectometry of LAO/STO heterostructures. (a) Experimental geometry for the reflectometry measurements, where the photon polarization is either within (π) or perpendicular to (σ) the scattering plane. Specific geometries are characterized by either the reflection angle θ or the photon momentum transfer in the z direction, q_z . (b) The graphic depicts orbital and electronic reconstructions at the interface via the orbital symmetry and opacity, respectively. For each atomic layer with a given orbital occupation, there exist isotropic and dichroic resonant scattering responses shown, which then combine to determine the reflectivity response of the material. (c, d) Simulated reflectivity maps for π -polarized light and energies spanning the Ti $L_{2,3}$ resonance on a 10 u.c. LAO/STO heterostructure in the case of no reconstructions (c), and combined orbital and electronic reconstructions (d).

charge than expected from electronic reconstruction [5]. More recent studies have shed some light on this issue, showing that a certain amount of charge is localized and thus hidden to transport measurements [23,24].

In addition to the total charge and its confinement profile near the interface, a crucial characteristic of the 2DEL is its orbital symmetry, which directly controls the mobility of the electrons and contributes to the energetic landscape of magnetism and superconductivity [6,8]. The interface electrons reside in the Ti $3d$ t_{2g} band, which is split into d_{xy} and $d_{xz/yz}$ subbands due to the tetragonal symmetry breaking imposed by the interface. First-principles calculations predict that the d_{xy} bands are lower in energy near the interface and thus host the majority of the charge, whereas $d_{xz/yz}$ bands become more occupied further from the interface [25–27]. X-ray absorption spectroscopy (XAS) experiments have verified this qualitatively, as linear dichroism measurements agree with the presence of lower energy d_{xy} orbitals [28]. However, the magnitude of this orbital reconstruction, and its spatial dependence moving away from the interface, have yet to be determined.

Here we study the electronic structure of the LAO/STO interface using synchrotron-based resonant x-ray reflectometry (RXR). RXR is the union of two powerful, complementary techniques: XAS, which probes the element-specific electronic structure (in particular the local $3d$ orbital occupations) through core-valence resonant electronic excitation, and reflectivity, which inherently contributes excellent interface and

depth sensitivity while also providing a natural quantitative detection scheme [29,30]. This combination of capabilities allows us to study the microscopic electronic structure properties specific to the 2DEL at the interface in exceptional detail. Previous studies on LAO/STO superlattices utilized a qualitative analysis of limited data sets to study electronic and orbital reconstructions [31,32]. Here we leverage the full power of RXR via a fully quantitative analysis of large data sets. In an extensive set of experiments, we apply RXR to LAO/STO samples below and above critical thickness for 2DEL formation and before and after annealing in an O_2 environment to eliminate potential oxygen vacancies, showing how orbital and electronic reconstruction define the spontaneous 2DEL formation.

In Figure 1(a) we depict the RXR experiment, showing the typical geometry for our reflection measurements using linearly polarized synchrotron x-rays. By changing the reflection angle or energy, one changes the momentum transfer q_z , leading to different interference effects (partial cancellation or enhancement of waves reflecting at different depths) and different interface sensitivity. Figure 1(b) shows via simulations the origin of reconstruction sensitivity in RXR. For the atomic planes near the interface exhibiting a particular reconstruction effect (where in the inset we depict orbital reconstructions via schematic orbital symmetries and electronic reconstructions via the opacity of the orbitals), the Ti atoms have very specific and different resonant scattering characteristics. Both the isotropic and the linear-dichroic responses of the scattering

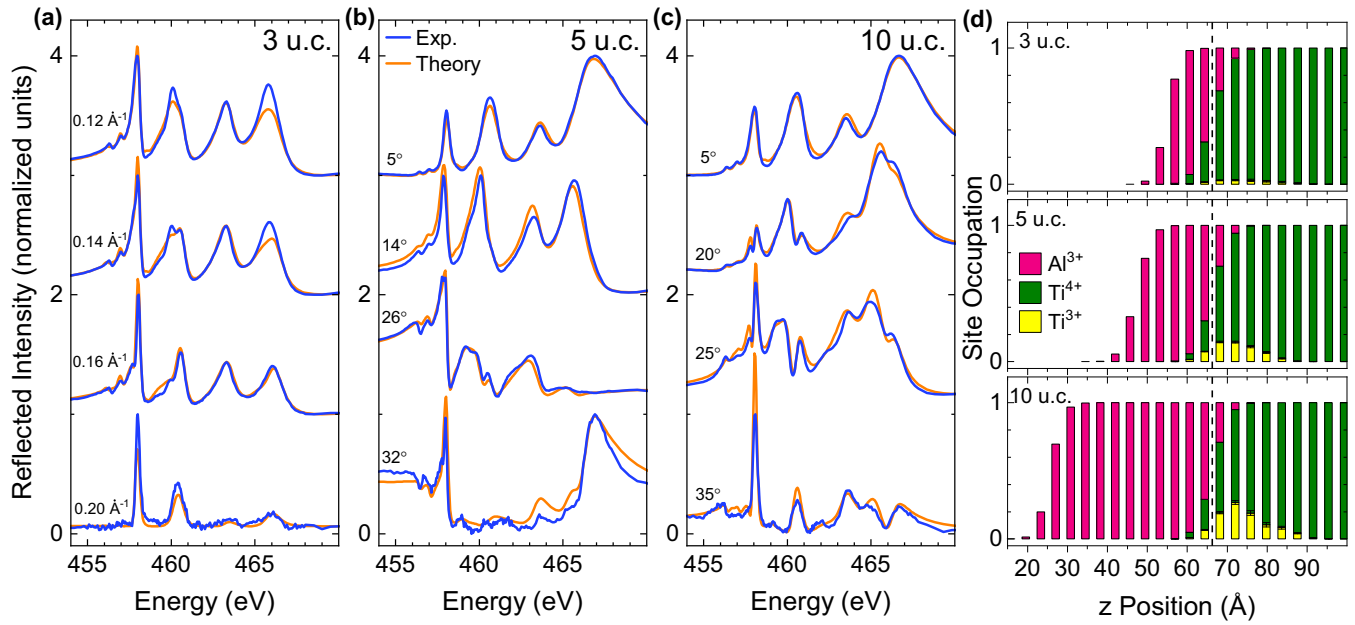


FIG. 2. Resonant reflectometry data and extracted charge profile for as-grown LAO/STO. (a–c) Experimental and modeled π -polarized energy scans across the Ti resonance at indicated fixed momentum transfer values or reflection angles for (a) 3 u.c., (b) 5 u.c., and (c) 10 u.c. samples. (d) B-site cation concentrations and 2DEL charge depth profile near the interface. Each vertical bar represents an atomic layer, so the distance between each pair is 1 u.c. The dashed vertical lines denote the approximate interface where equal amounts of Ti and Al are found. Extended data sets and simulation results can be found in the Supplemental Material [34].

show strong dependences on orbital occupation at these Ti $L_{2,3}$ resonance energies.

The resonant atomic scattering responses combine to yield the electric susceptibility of the material, and thus a particular reconstruction at the interface leads to a specific reflectivity response, which we investigate with model data in Figs. 1(c) and 1(d). Here the predicted RXR for a 10 u.c. LAO/STO sample is shown for energies spanning the Ti $L_{2,3}$ resonance and reflection angles spanning a typical measurable range [33]. Note we multiply the reflectivity spectra here by q_z^4 in order to show a wide q_z range where the intensity spans several orders of magnitude. As shown by the two plots, at high-momentum transfers, very pronounced effects are expected in the RXR data due to orbital and electronic reconstructions, even if they are confined to only 2 u.c. near the buried interface as in the realistic example simulated here. This strong sensitivity, and the quantitative nature of RXR, make this technique very useful for studying oxide interfaces.

We have applied RXR to a series of samples to perform a comprehensive study of the LAO/STO reconstruction phenomena. Figure 2 details the reflectivity data and analysis results for samples having LAO thicknesses of 3, 5, and 10 u.c. Figures 2(a)–2(c) show selected reflectivity data along with model fit results (complete data sets are presented in the Supplemental Material [34]). Signatures of the thickness-dependent onset of the 2DEL are immediately evident from the data, as the 3 u.c. sample exhibits a less featured reflectivity response similar to that in Fig. 1(c), whereas the spectra of the thicker samples reveal a much more detailed structure, comparable to that in Fig. 1(d).

We model the depth-dependent electric susceptibility of the heterostructures starting from the atomic level, where the

Ti resonant scattering response is computed using quantum many-body theory [35,36], while the off-resonant scattering responses of all atoms are taken from tabulated data [37]. The resonant response depends strongly on the local 3d orbital occupation of the Ti atoms, thus providing the sensitivity to the 2DEL density and symmetry. From the susceptibility we compute the energy- and angle-dependent reflectivity response and fit the material parameters as described in the Methods section. The fit results are overlaid with the experimental data in Figs. 2(a)–2(c), where an excellent level of agreement is evident. The models corresponding to these fits, which quantify the interfacial reconstruction phenomena, are shown in Fig. 2(d) and Fig. 3. In Fig. 2(d) we plot fractional atomic site occupations for the cations in the samples (full concentration profiles, including anions, are presented in the Supplemental Material [34]), where our resonant Ti analysis allows us to distinguish between Ti⁴⁺ and Ti³⁺ valences (i.e., the respective absence or presence of the 2DEL charge). Evident is the ~ 1 –2 u.c. average roughness at both the surface and the interface, comparable to that found with other techniques [21,38,39]. Strong evidence is present for the 4 u.c. threshold for 2DEL formation, as the 3 u.c. sample is found to have significantly less charge than the thicker samples. As shown in Table I, for the 3 u.c. sample our fit converges with a small amount of charge at 0.16 e^- /u.c. This charge is distributed rather evenly over 4 nm near the interface, whereas the thicker samples have much more pronounced concentrations confined to the interface. The total charge quantities in the 5 and 10 u.c. samples are significant, as also shown in Table I.

In Fig. 3, the extracted interface-induced symmetry breaking of the Ti 3d orbitals is detailed. While the 3d orbitals have O_h symmetry in the bulk of the STO, the presence of the

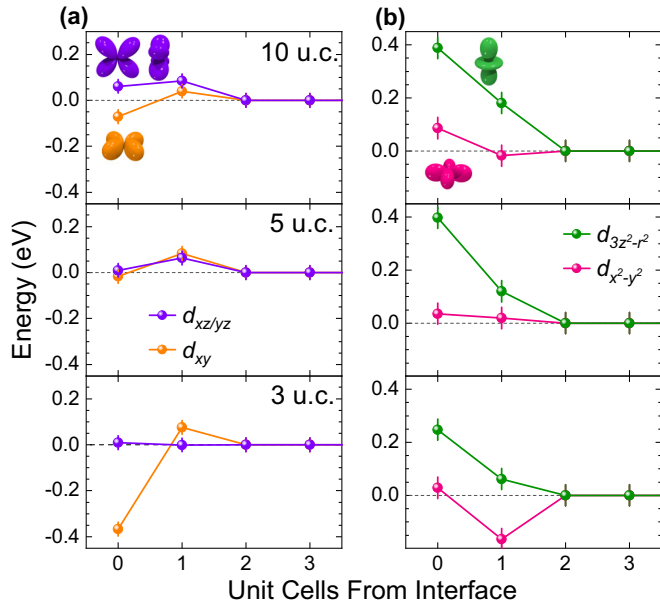


FIG. 3. Orbital reconstruction of as-grown LAO/STO quantified via reflectometry. (a) The t_{2g} and (b) e_g orbital energies for the Ti atomic layers near the LAO/STO interface, relative to the bulk orbital energies.

interface leads to a tetragonal local symmetry distortion [28]. By computing the tetragonally symmetric Ti resonant scattering tensor according to the energies of the $3d$ orbitals, and fitting to our polarization-dependent RXR spectra, we can extract the depth dependence of the orbital energies relative to those of the bulk. For all samples (regardless of 2DEL presence), we detect a strong symmetry breaking in the 2 u.c. closest to the interface. We find the d_{xy} orbital to be lowest in energy near the interface, as predicted by first-principles modeling [25,26] and qualitatively observed experimentally [28]. Further, we detect that the tetragonal distorting of orbital energies is enhanced in the presence of the 2DEL, a feature also previously predicted from first principles [27]. Given the different effective masses for d_{xy} versus $d_{xz/yz}$ carriers, a detailed quantification of this orbital symmetry breaking is key to understanding the comprehensive transport properties of the LAO/STO system.

While a common observation in many experimental studies is that the 2DEL total charge is much less than the $0.5 e^-$ per square u.c. predicted by the polar catastrophe model [5], we find here quantities relatively close to this value—in fact they are systematically slightly higher. Oxygen vacancies (either in the LAO film or in the STO substrate) can be an electron

TABLE I. Total charge hosted in the Ti $3d$ orbitals near the interface for each sample, as extracted from the RXR fits.

Sample	Charge ($e^-/\text{u.c.}$)
3 u.c.	0.16 ± 0.03
5 u.c.	0.59 ± 0.05
10 u.c.	0.97 ± 0.08
10 u.c. (annealed)	0.50 ± 0.03

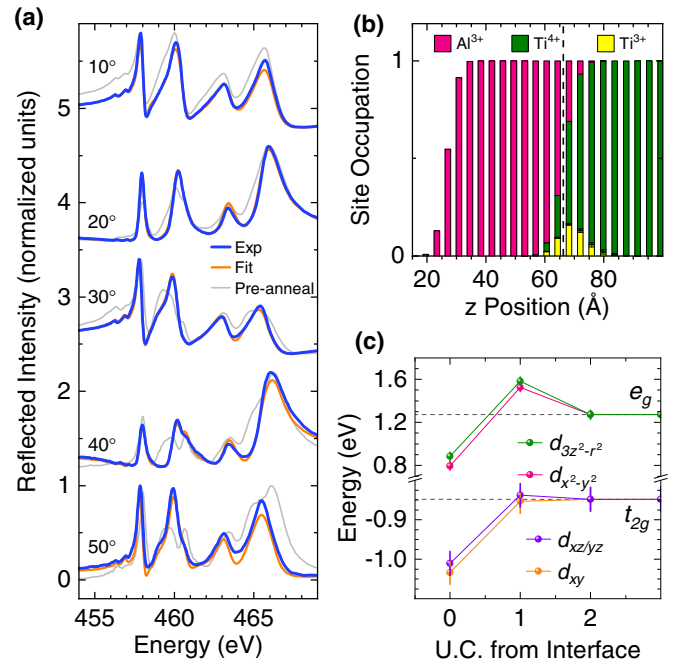


FIG. 4. Effects of postgrowth oxygen annealing. (a) Experimental and modeled fixed angle, σ -polarized, reflectometry scans across the Ti resonance are shown for a 10 u.c. LAO/STO after annealing in an O_2 environment. The experimental data for the same sample before annealing are shown in gray for comparison. (b) 2DEL charge profile after annealing. (c) Orbital energies after annealing, extracted from the reflectometry analysis.

dopant, leading to excess carriers in the 2DEL as well as electron trapping [40]. To investigate the possible effect of oxygen vacancies, we measured an RXR data set on the same 10 u.c. sample, immediately after annealing in a partial pressure (200 mbar) O_2 environment. The results, shown in Fig. 4, display a significant change in the RXR response on annealing, indicating a strong sensitivity of RXR to the oxygen content and corresponding Ti charge variation. The data and model fits are shown in Fig. 4(a), with the preannealing data plotted as well for comparison. Performing the same quantitative analysis for this case, we find that the charge density is reduced from $0.97 e^-/\text{u.c.}$ down to a postannealed value of $0.50 \pm 0.03 e^-/\text{u.c.}$, in agreement with the predicted value of $0.5 e^-/\text{u.c.}$ within our fitting uncertainty. This decrease in 2DEL total charge is consistent with what we observe in transport measurements (see Supplemental Material [34]). The charge profile is plotted in Fig. 4(b), where it is evident the total charge decreases postannealing and also becomes more confined to the interface (without considering interface broadening, the mean 2DEL charge depth is 0.4 u.c. past the first TiO_2 layer postannealing versus 1.5 u.c. before). Finally, in Fig. 4(c) we show the postannealing orbital energy profiles. Interestingly, the orbital energies after annealing exhibit a much weaker tetragonal splitting (23 versus 133 meV), suggesting that the larger orbital splittings for the 10 u.c. sample prior to annealing in Fig. 3 could be due primarily to strong potential variations due to oxygen vacancies [41]. Further, the d_{xy} orbital is shifted to a lower energy at the interface postannealing, explaining the tighter confinement of the 2DEL charge.

Our resonant x-ray reflectivity analysis of the LAO/STO 2DEL provides crucial answers to questions regarding oxide interface reconstruction phenomena. We find total charge quantities consistent with the theory of polarity-induced electronic reconstruction, elucidate the effects of oxygen vacancies on this system, and further extract the confinement profile of the reconstructed charge. Additionally, the RXR technique allows us to quantify the orbital symmetry of electronic states at Angstrom length scales, showing that significant symmetry breaking effects of the Ti $3d$ orbitals are confined to within 2 u.c. of the interface. Crucially, the nature of RXR allows us to probe the entire reconstructed charge density, not just mobile carriers. Building on the results presented here, future RXR experiments will be helpful to closely examine the 4 u.c. threshold for 2DEL formation, as well as O_2 annealing of samples of various thicknesses. Additionally, with such a precise quantification of the 2DEL characteristics, future efforts can be directed toward engineering these properties for the development of functional devices, either in the LAO/STO system or in the other oxide heterostructures. Finally, while these findings are important for the understanding of the LAO/STO electronic system and related oxide reconstruction phenomena, our results also show resonant x-ray reflectivity to be an invaluable tool for the burgeoning field of oxide interfaces.

II. METHODS

The set of samples investigated included 3, 5, and 10 u.c. LAO films grown by pulsed laser deposition on TiO_2 -terminated $SrTiO_3$ substrates. A KrF excimer laser operating at 248 nm was used, with a fluence of 1 J/cm² and repetition rate of 1 Hz. The growth took place at 800 °C in an O_2 pressure of 1×10^{-3} mbar. After deposition, all samples were cooled down in a higher O_2 pressure of 5×10^{-3} mbar at a rate of 30 °C/min. Atomic layer growth was controlled using reflection high-energy electron diffraction, as reported in the Supplemental Material [34]. Postannealed samples were annealed at a temperature of 530 °C under an O_2 pressure of 200 mbar for 1 h.

The RXR experiments were carried out at the REIXS beamline of the Canadian Light Source [42] at 300 K in an ultrahigh vacuum environment ($<10^{-9}$ mbar). Reflection intensity was monitored using a filtered photodiode, whose response function was measured using the direct synchrotron beam. Data were normalized by the incident beam flux and the photodiode response to obtain the quantitative reflectivity spectra. Two different measurement modes were used for data presented in this work. For data in Fig. 2(a), the momentum

transfer was held fixed by slightly varying the reflection angle for each energy. For all other data the reflection angle was held fixed while varying incident energy. Either mode can be used for a successful RXR analysis, provided a sufficient sampling of the energy versus angle/momentum space is made.

Simulations of the Ti $L_{2,3}$ resonant response for given orbital energies and occupations were carried out with multiplet crystal field theory. This model Hamiltonian approach includes the full multiplet effects arising from strong atomic Coulomb interactions, as well as crystal field perturbations arising from the bonding with oxygen. Exact diagonalization and simulations of the spectral functions were carried out with the software *Quanty* [35,36,43,44]. The simulated resonances were merged with tabulated off-resonant atomic scattering factors f_2 [37], and the scattering factors f_1 were then calculated from the Kramers-Kronig relations. For all other elements (La, Sr, O, Al), off-resonant tabulated scattering factors were used. With all atomic scattering factors determined, the reflectivity was simulated and fit to the experiment using the dynamical diffraction software QUAD [45].

ACKNOWLEDGMENTS

This work was supported by the Natural Sciences and Engineering Research Council of Canada, the Canadian Institute for Advanced Research, the Max Planck-UBC-UTokyo Centre for Quantum Materials, and the Canada First Research Excellence Fund, Quantum Materials and Future Technologies Program. Team members from the University of Würzburg were supported by the Deutsche Forschungsgemeinschaft (DFG), Project-ID 258499086-SFB 1170. Team members from the University of Twente were supported by the Netherlands Organization for Scientific Research (NWO). Part of the research described in this paper was performed at the Canadian Light Source, a national research facility of the University of Saskatchewan, which is supported by the Canada Foundation for Innovation (CFI), the Natural Sciences and Engineering Research Council of Canada, the National Research Council (NRC), the Canadian Institutes of Health Research (CIHR), the Government of Saskatchewan, and the University of Saskatchewan. We thank Research Computing at the University of Saskatchewan for computational resources.

Resonant reflectivity experiments were performed by R.J.G., S.M., R.S., and F.H. Data analysis was performed by R.J.G. with contributions from V.Z., M.Z., S.M., J.G., V.H., and G.A.S. Sample synthesis and initial characterization was managed and carried out by Z.L., M.H., G.R., and G.K. The manuscript was written by R.J.G. with input from all authors.

-
- [1] D. Khomskii, *Transition Metal Compounds* (Cambridge University Press, Cambridge, England, 2014).
 [2] J. Mannhart and D. G. Schlom, *Science* **327**, 1607 (2010).
 [3] H. Y. Hwang, Y. Iwasa, M. Kawasaki, B. Keimer, N. Nagaosa, and Y. Tokura, *Nature Mater.* **11**, 103 (2012).
 [4] A. Ohtomo and H. Hwang, *Nature (London)* **427**, 423 (2004).

- [5] S. Thiel, G. Hammerl, A. Schmehl, C. W. Schneider, and J. Mannhart, *Science* **313**, 1942 (2006).
 [6] N. Manca, D. Bothner, A. M. R. V. L. Monteiro, D. Davidovikj, Y. G. Sağlam, M. Jenkins, M. Gabay, G. A. Steele, and A. D. Caviglia, *Phys. Rev. Lett.* **122**, 036801 (2019).

- [7] Y.-Y. Pai, H. Lee, J.-W. Lee, A. Annadi, G. Cheng, S. Lu, M. Tomczyk, M. Huang, C.-B. Eom, P. Irvin, and J. Levy, *Phys. Rev. Lett.* **120**, 147001 (2018).
- [8] T. V. Trevisan, M. Schütt, and R. M. Fernandes, *Phys. Rev. Lett.* **121**, 127002 (2018).
- [9] H. Thierschmann, E. Mulazimoglu, N. Manca, S. Goswami, T. M. Klapwijk, and A. D. Caviglia, *Nat. Commun.* **9**, 2276 (2018).
- [10] N. Reyren, S. Thiel, A. D. Caviglia, L. F. Kourkoutis, G. Hammerl, C. Richter, C. W. Schneider, T. Kopp, A.-S. Ruetschi, D. Jaccard, M. Gabay, D. A. Muller, J.-M. Triscone, and J. Mannhart, *Science* **317**, 1196 (2007).
- [11] L. Li, C. Richter, J. Mannhart, and R. C. Ashoori, *Nat. Phys.* **7**, 762 (2011).
- [12] F. Zhang, P. Lv, Y. Zhang, S. Huang, C.-M. Wong, H.-M. Yau, X. Chen, Z. Wen, X. Jiang, C. Zeng, J. Hong, and J.-y. Dai, *Phys. Rev. Lett.* **122**, 257601 (2019).
- [13] D.-S. Park, A. Rata, I. Maznichenko, S. Ostanin, Y. Gan, S. Agrestini, G. Rees, M. Walker, J. Li, J. Herrero-Martin *et al.*, *Nat. Commun.* **11**, 3650 (2020).
- [14] A. Brinkman, M. Huijben, M. Van Zalk, J. Huijben, U. Zeitler, J. C. Maan, W. G. Van der Wiel, G. Rijnders, D. H. A. Blank, and H. Hilgenkamp, *Nature Mater.* **6**, 493 (2007).
- [15] J. A. Bert, B. Kalisky, C. Bell, M. Kim, Y. Hikita, H. Y. Hwang, and K. A. Moler, *Nat. Phys.* **7**, 767 (2011).
- [16] M. Breitschaft, V. Tinkl, N. Pavlenko, S. Paetel, C. Richter, J. R. Kirtley, Y. C. Liao, G. Hammerl, V. Eyert, T. Kopp, and J. Mannhart, *Phys. Rev. B* **81**, 153414 (2010).
- [17] U. Khanna, P. K. Rout, M. Mograbi, G. Tuvia, I. Leermakers, U. Zeitler, Y. Dagan, and M. Goldstein, *Phys. Rev. Lett.* **123**, 036805 (2019).
- [18] M. Briggeman, J. Li, M. Huang, H. Lee, J.-W. Lee, K. Eom, C.-B. Eom, P. Irvin, and J. Levy, *Sci. Adv.* **6**, eaba6337 (2020).
- [19] M. Briggeman, M. Tomczyk, B. Tian, H. Lee, J.-W. Lee, Y. He, A. Tylan-Tyler, M. Huang, C.-B. Eom, D. Pekker, R. S. K. Mong, P. Irvin, and J. Levy, *Science* **367**, 769 (2020).
- [20] A. Geondzhian, A. Sambri, G. M. De Luca, R. Di Capua, E. Di Gennaro, D. Betto, M. Rossi, Y. Y. Peng, R. Fumagalli, N. B. Brookes, L. Braicovich, K. Gilmore, G. Ghiringhelli, and M. Salluzzo, *Phys. Rev. Lett.* **125**, 126401 (2020).
- [21] N. Nakagawa, H. Y. Hwang, and D. A. Muller, *Nat. Mater.* **5**, 204 (2006).
- [22] R. Hesper, L. H. Tjeng, A. Heeres, and G. A. Sawatzky, *Phys. Rev. B* **62**, 16046 (2000).
- [23] M. Sing, G. Berner, K. Goß, A. Müller, A. Ruff, A. Wetscherek, S. Thiel, J. Mannhart, S. A. Pauli, C. W. Schneider, P. R. Willmott, M. Gorgoi, F. Schäfers, and R. Claessen, *Phys. Rev. Lett.* **102**, 176805 (2009).
- [24] T. C. Asmara, A. Annadi, I. Santoso, P. K. Gogoi, A. Kotlov, H. M. Omer, M. Motapothula, M. B. H. Breese, M. Ruebhausen, T. Venkatesan, Ariando, and A. Rusydi, *Nat. Commun.* **5**, 3663 (2014).
- [25] Z. S. Popović, S. Satpathy, and R. M. Martin, *Phys. Rev. Lett.* **101**, 256801 (2008).
- [26] W.-j. Son, E. Cho, B. Lee, J. Lee, and S. Han, *Phys. Rev. B* **79**, 245411 (2009).
- [27] S. Stemmer and S. James Allen, *Annu. Rev. Mater. Res.* **44**, 151 (2014).
- [28] M. Salluzzo, J. C. Cezar, N. B. Brookes, V. Bisogni, G. M. De Luca, C. Richter, S. Thiel, J. Mannhart, M. Huijben, A. Brinkman, G. Rijnders, and G. Ghiringhelli, *Phys. Rev. Lett.* **102**, 166804 (2009).
- [29] S. Macke, A. Radi, J. E. Hamann-Borrero, A. Verna, M. Bluschke, S. Brck, E. Goering, R. Sutarto, F. He, G. Cristiani, M. Wu, E. Benckiser, H.-U. Habermeier, G. Logvenov, N. Gauquelin, G. A. Botton, A. P. Kajdos, S. Stemmer, G. A. Sawatzky, M. W. Haverkort *et al.*, *Adv. Mater.* **26**, 6554 (2014).
- [30] S. Macke and E. Goering, *J. Phys.: Condens. Matter* **26**, 363201 (2014).
- [31] H. Wadati, D. G. Hawthorn, J. Geck, T. Higuchi, Y. Hikita, H. Y. Hwang, L. F. Kourkoutis, D. A. Muller, S.-W. Huang, D. J. Huang, H.-J. Lin, C. Schler-Langeheine, H.-H. Wu, E. Schierle, E. Weschke, N. J. C. Ingle, and G. A. Sawatzky, *J. Appl. Phys.* **106**, 083705 (2009).
- [32] J. Park, B.-G. Cho, K. D. Kim, J. Koo, H. Jang, K.-T. Ko, J.-H. Park, K.-B. Lee, J.-Y. Kim, D. R. Lee, C. A. Burns, S. S. A. Seo, and H. N. Lee, *Phys. Rev. Lett.* **110**, 017401 (2013).
- [33] Note we multiply the reflectivity spectra here by q_z^4 in order to show a wide q_z range where the intensity spans several orders of magnitude.
- [34] See Supplemental Material at <http://link.aps.org/supplemental/10.1103/PhysRevMaterials.5.065004> for details on sample growth, reflectometry experiments, and reflectometry modelling, as well as extended datasets and analysis results for all samples.
- [35] M. W. Haverkort, M. Zwierzycki, and O. K. Andersen, *Phys. Rev. B* **85**, 165113 (2012).
- [36] M. W. Haverkort *et al.*, <http://www.quanty.org>.
- [37] B. Henke, E. Gullikson, and J. Davis, *At. Data Nucl. Data Tables* **54**, 181 (1993).
- [38] P. R. Willmott, S. A. Pauli, R. Herger, C. M. Schlepütz, D. Martoccia, B. D. Patterson, B. Delle, R. Clarke, D. Kumah, C. Cionca, and Y. Yacoby, *Phys. Rev. Lett.* **99**, 155502 (2007).
- [39] S. A. Chambers, M. H. Engelhard, V. Shutthanandan, Z. Zhu, T. C. Droubay, L. Qiao, P. Sushko, T. Feng, H. D. Lee, T. Gustafsson, *et al.*, *Surf. Sci. Rep.* **65**, 317 (2010).
- [40] C. Yin, A. E. M. Sminck, I. Leermakers, L. M. K. Tang, N. Lebedev, U. Zeitler, W. G. van der Wiel, H. Hilgenkamp, and J. Aarts, *Phys. Rev. Lett.* **124**, 017702 (2020).
- [41] N. Pavlenko, T. Kopp, E. Y. Tsymal, J. Mannhart, and G. A. Sawatzky, *Phys. Rev. B* **86**, 064431 (2012).
- [42] D. G. Hawthorn, F. He, L. Venema, H. Davis, A. J. Achkar, J. Zhang, R. Sutarto, H. Wadati, A. Radi, T. Wilson, G. Wright, K. M. Shen, J. Geck, H. Zhang, V. Novk, and G. A. Sawatzky, *Rev. Sci. Instrum.* **82**, 073104 (2011).
- [43] Y. Lu, M. Höppner, O. Gunnarsson, and M. W. Haverkort, *Phys. Rev. B* **90**, 085102 (2014).
- [44] M. W. Haverkort, G. Sangiovanni, P. Hansmann, A. Toschi, Y. Lu, and S. Macke, *Europhys. Lett.* **108**, 57004 (2014).
- [45] S. Macke, J. E. Hamann-Borrero, R. J. Green, B. Keimer, G. A. Sawatzky, and M. W. Haverkort, *Phys. Rev. Lett.* **117**, 115501 (2016).